

# Paraffin-based and metal-loaded HTPB fuel regression-rates study in a lab-scale hybrid rocket fed with N<sub>2</sub>O

*F. Scaramuzzino\**, *C. Carmicino\*\**, *G. Festa\*\**, *A. Viviani\** and *A. Russo Sorge\*\**

\* *Dipartimento di Ingegneria Industriale e dell'Informazione, Seconda Università di Napoli, Italy*

[francesca.scaramuzzino@unina2.it](mailto:francesca.scaramuzzino@unina2.it)

\*\* *Dipartimento di Ingegneria Industriale, Università di Napoli "Federico II", Italy*

[carmicin@unina.it](mailto:carmicin@unina.it)

## Abstract

In the effort of increasing the notoriously slow fuel-regression rate of hybrid rockets two approaches are investigated in this paper: addition of metal particles in HTPB grains against the use of paraffin-based fuels, which are expected to raise significantly the regression rate.

A series of firing tests on two lab-scales hybrid rocket engines have been carried out with gaseous nitrous oxide and pure HTPB, aluminum-loaded HTPB or paraffin wax. Scale effects are examined. Outcomes are discussed in terms of regression rate and combustion efficiency. A comparison with the data retrieved from pure HTPB or metal-loaded HTPB burnt with gaseous oxygen is also drawn. Both aluminum powder addition to HTPB and the use of paraffin-based fuel appear to increase regression rate, the latter showing the major gain. In particular aluminum powder addition seems to increase regression rate more than observed with oxygen.

## NOMENCLATURE

$\dot{m}_{ent}$	=	entrainment component of mass flux from fuel surface	$\bar{D}$	=	fuel port mean diameter
$P_d$	=	dynamic pressure	$\Delta M$	=	fuel mass loss
$h$	=	thickness of the melt layer at the fuel surface	$t_b$	=	combustion time
$\sigma$	=	surface tension	$D_0$	=	initial fuel port diameter
$\mu_l$	=	cinematic viscosity of melt layer	$D_2$	=	final fuel port diameter
$A_{throat}$	=	nozzle throat area	$G$	=	total mass flux
$\bar{r}$	=	average regression rate	$G_{ox}$	=	oxygen mass flux
$\bar{m}_f$	=	average fuel mass flow rate	$C^*$	=	characteristic exhaust velocity
$\bar{m}_{ox}$	=	average oxygen mass flow rate	$\eta C^*$	=	combustion efficiency
$L$	=	grain length	O/F	=	mixture ratio
$\rho_f$	=	fuel density	$P_{aft}$	=	aft-chamber pressure
			$P_c$	=	chamber pressure
			$P_{feed}$	=	oxygen feeding pressure

## 1. Introduction

The hybrid rocket is a kind of green and safe chemical propulsion system. Its inherent safety is a direct consequence of the storage of fuel and oxidizer in different phases. In the most common configuration, a liquid or gaseous oxidizer and a solid-fuel grain are employed. Beside safety, on the one hand hybrid engines show some interesting features provided by both conventional solid and liquid propellant rockets offering advantages such as reliability, throttle-ability and re-ignition but, on the other, hybrids using classical polymeric fuels suffer from slow regression rate and, in general, relatively poor combustion efficiency.

The low fuel regression rate is a consequence of the heat and mass transfer mechanisms involved from the flame to the fuel surface. Figure 1 shows the distinctive combustion process occurring in hybrid rockets. The boundary layer is formed on the fuel wall due to the oxidizer injection into the fuel grain port. Combustion develops inside the layer, where oxidizer and gasified fuel react. The diffusive flame is located relatively far from the fuel surface and it is fed, from the outer side, by the oxidizer stream and, from the inner side, by the products of fuel pyrolysis, which is sustained by the flame itself. Fuel surface blowing decreases the velocity gradient at the surface, thus reducing the convective heat transfer by means of the so-called blocking effect [1].

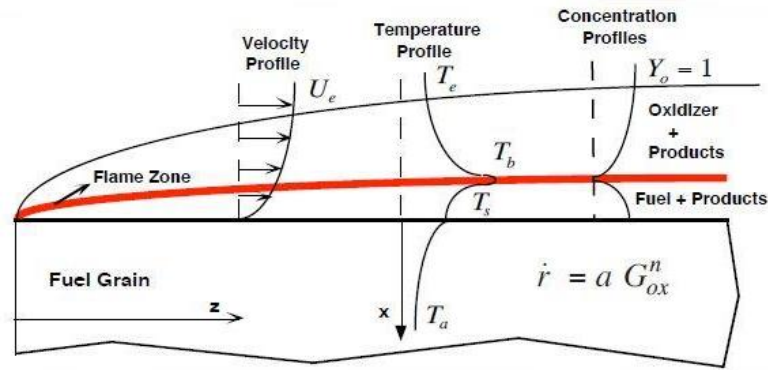


**Figure 1: Combustion scheme of hybrid rocket**

Several methods have been studied and applied more or less recently with the aim to improve the fuel regression rate making the hybrid engine a viable contender of solid and liquid rockets in a number of space missions. In the present paper two particular techniques are investigated:

- *Addition of metal additives in the pure fuel*  
Mainly, high-energy fuel ingredients, such as metals and metal hydrides, can enhance heat release near the regression surface improving the heat feedback and, therefore, the regression rate of the solid grain.
- *Paraffin-fuel grain casting*  
Paraffin grains mostly regress involving a mass-transfer mechanism that does not rely only on the heat transfer from the flame, overcoming the diffusion-limited process and the blocking effect.

After a brief discussion about the details of the two aforementioned approaches, results of a series of static firings of two laboratory hybrid rocket engines (one in the class of 0.2-kN thrust and one in the class of 1 kN) burning nitrous oxide with different solid-fuel compositions, such as paraffin-based and aluminum-loaded HTPB grains, are presented in this work. Experimental tests have been carried out through two national projects; in particular tests involving paraffin grains have been developed in collaboration with Politecnico di Milano with the financial support of Italian Ministry PRIN2009; whereas, HTPB grains with aluminum have been produced by AVIO in the framework of THESEUS program. Regression rate and combustion efficiency are reported and compared to the ones obtained burning the same propellants with gaseous oxygen (see Ref. [2] and [3]).

## 2. Bases of regression rate improvement techniques

Combustion of metals, thanks to their large heat of reaction and high density, shows in principle inherent advantages. The technique of metal powders addition to conventional fuels has been widely investigated in the past as a means to increase both the fuel mass flow rate and the specific impulse compared to pure fuel. Since 60', researchers have observed a regression rate improvement consequent on the addition of aluminum or of other metal powders to the fuel grain [4]. Strand et al. [5] supported the inclusion of particulate additives (aluminum and/or coal) in solid fuels as an approach to enhance fuel regression rate. In fact, the blocking effect depends only on the gas blowing rate. The density of the volatile fuel mass flow is

$$\rho_v = (1 - k)\rho_f \quad (1)$$

where  $k$  is the weight fraction of added metal particles. Thus the blocking effect is expected to be reduced and the regression rate to be raised proportionally to the factor  $(1 - k)^{-1}$ . Furthermore also the decrease of effective heat of gasification, due to the non-volatile particle heating, and the increased radiation heat flux should contribute to the regression rate improvement. In addition, the flame temperature is increased contributing to the regression rate enhancement though on a lower extent [6].

Several energetic powders have been considered and tested in the framework of the Operative Research Project on Hybrid Engine in Europe (ORPHEE) (see [3] and [7]), such as nano-sized aluminum, nano-sized Viton-coated aluminum, magnesium hydride, magnesium, nano-sized iron or iron and magnesium. Nevertheless, results obtained in the experimental campaign with pure HTPB loaded with these different particles have demonstrated that regression rate is not significantly improved by the addition of powders compared to pure fuel.

In the last years, research has focused on paraffin-based fuels.

Researchers at Stanford University [8] have demonstrated that this kind of fuel displays regression rate up to 3-4 times higher than conventional hybrid fuels.

The intrinsic characteristic of paraffin-based fuels is the onset of a thin liquid layer on the fuel grain surface which may become unstable, as shown in Figure 2. In fact, due to the low viscosity and surface tension, it is affected by an instability driven by the oxidizer flow. This instability leads to the lift-off and entrainment of fuel droplets into the main gas stream, increasing the fuel mass transfer rate. This mass-transfer mechanism, like a continuous spray injection spanned along the grain port, does not depend on heat transfer and raises the fuel mass flow avoiding the blocking effect typical of gaseous fuel blowing.

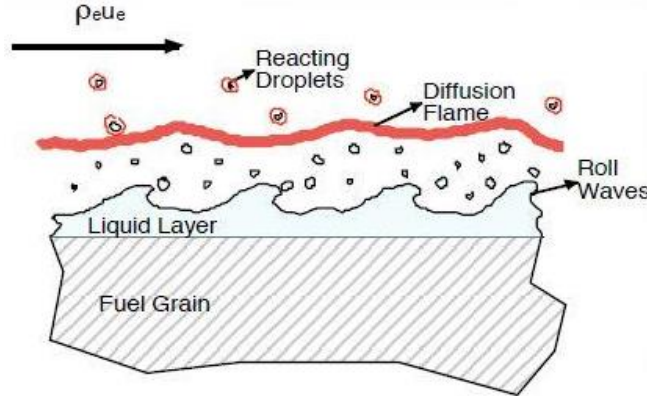


**Figure 2: Combustion scheme of a liquefying fuel hybrid rocket**

The entrainment component of fuel regression rate has been demonstrated to depend on the parameters shown in the Eq. (2)

$$\dot{m}_{ent} \propto \frac{P_d^\alpha h^\beta}{\sigma^\pi \mu_l^\gamma} \quad (2)$$

The entrained mass flow depends directly on dynamic pressure,  $P_d$ , and layer thickness  $h$ . The entrainment occurs only when the liquid in the melt layer has low values of viscosity,  $\mu$ , and surface tension,  $\sigma$ , both evaluated at the characteristic temperature of the layer. The experimental data suggest that the dynamic pressure exponent,  $\alpha$ , is in the range of 1-1.5. For example Gater and L'Ecuyer [9], scaling for large mass fluxes, indicate that  $\alpha$  is approximately 1.5 and  $\beta$  is equal to 2. The viscosity and surface tension exponents, respectively  $\pi$  and  $\gamma$  are both predicted to be 1. The normal-alkane class of hydrocarbons with carbon number greater than 14 and solid phase at standard conditions have a low surface tension and viscosity at the melt layer conditions typical of hybrid rockets. These propellants, including paraffin, are envisaged to raise considerably the regression rate compared to conventional hybrid propellants [8] and [10].

### 3. Experimental set-up

A scheme of the smaller lab-scale rocket engine employed in the current test campaign is depicted in Figure 3.

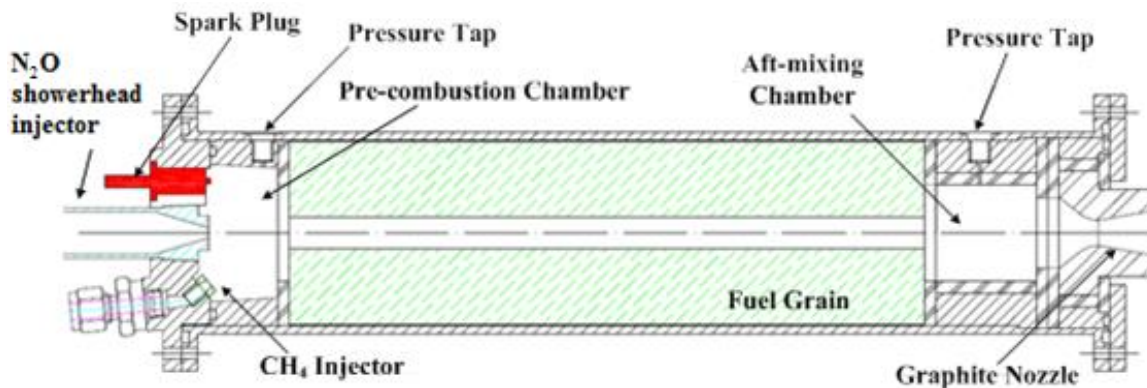


**Figure 3: Lab-scale hybrid motor scheme**

The lab-scale motor has an axisymmetric combustion chamber, with 350-mm length and 69.2-mm inner case diameter. This motor is in the class of 0.2-kN thrust and is set up on a test stand capable of handling a larger motor as well, in the class of 1 kN (for the details see also [11]).

The smaller motor has been selected to properly accommodate the smaller paraffin-fuel grains supplied by the SPLab of Politecnico di Milano ([12] and [13]).

The oxidizer is nitrous oxide; it is supplied by a reservoir of 10 cylinders from which it is delivered in gaseous phase with an upstream pressure approximately about 40 bar.

The cylinder rack is connected to the motor feeding line with an electronically controlled TESCOM pressure regulator.

Oxidizer mass flow rate is evaluated through gas temperature and pressure measurements across a sub-critical Venturi tube. A non-choked device is mandatory in order to avoid gas-to-liquid phase change, affecting the mass flow rate measurement. Temperature and pressure are acquired at a section upstream of the Venturi throat; starting from the latter parameters, density is calculated by means of the Redlich-Kwong-Soave equation of state. A differential pressure transducer is used to measure the pressure drop between the section upstream of the throat and the throat itself.

Oxidizer is axially injected into the combustion port through a showerhead injector with 13 holes with 1.1-mm diameter. Figure 4 displays the injection flange and the injector device.



**Figure 4: Injection flange and the showerhead injector device**

Nitrogen is also purged into the chamber for the burn out and in case of an accident.

Upstream and downstream of the fuel grain a dump plenum and an aft-mixing chamber are set up, respectively. The pre-chamber shifts towards the fore end of the grain the recirculation region caused by the oxidizer injection, in order to increase the overall regression rate. The aft-chamber, covered with thermal insulations, promotes additional gas mixing, thereby improving the combustion efficiency.

Graphite converging-diverging nozzles with either 9.6 or 12-mm throat diameter have been employed; the one with larger diameter has been selected to maintain chamber pressure in the allowable range for the combustion chamber (maximum estimated pressure around 30 bar).

The motor is suspended from the test bench by 4 load cells; this arrangement allows computing the motor thrust as the sum of the loads measured by each cell. Chamber pressure is measured by two capacitive transducers, Setra model C206, set up in the pre-chamber and in the aft-chamber.

A spark plug (powered by a Honeywell solid-state igniter spark generator) is arranged in the pre-chamber where methane gas is injected for 3 seconds together with the oxidizer to ignite the motor. This system has been set up in order to ensure repeatable conditions at the motor ignition as well as to guarantee motor re-ignition.

The analog signals coming from thermocouples, pressure transducers and load cells are sampled at 5 kHz, digitally converted, processed and recorded on the hard disk by a National Instruments (NI) SCXI system interconnected with the computer via a NI 6034 E PCI board with 16-bit resolution. With this equipment and using a software developed in *LabView*, the motor is ignited and the firing test is completely automated. All the signals are saved in a binary format for post-processing and in text format, after averaging down the data to 100 Hz ("boxcar averaging").

The time-space-averaged regression rate is simply calculated from the equation:

$$\bar{r} = \frac{\bar{m}_f}{\pi L \rho_f \bar{D}} \quad (3)$$

where  $L$  is the grain length and  $\rho_f$  is the fuel density;  $\bar{m}_f$  is the average fuel mass flow rate that is determined by dividing the fuel grain mass loss  $\Delta M$  by the burn time,  $t_b$ :

$$\bar{m}_f = \frac{\Delta M}{t_b} \quad (4)$$

$\bar{D}$  is the port diameter averaged over the entire burning, it is determined starting from the initial port diameter and the final average port diameter  $D_2$ , which is estimated by means of the fuel mass burned as follows:

$$D_2 = \sqrt{D_0 + \frac{4}{\pi} \frac{\Delta M}{\rho_f L}} \quad (5)$$

The burn time, which involves the identification of the initial surface regression and the web burnout instants, has been determined based on a well assessed procedure [14]. The inflection point on the primary rise portion of the pre-chamber pressure trace and the one on the end decrease portion are assumed, respectively, as these two characteristic times.

The time-space-averaged mass flux (whether it is the oxidizer or the total one) is defined based on the average port diameter  $\bar{D} = 0.5 (D_0 + D_2)$ :

$$G = 4 \frac{\bar{m}}{\pi \bar{D}^2} \quad (6)$$

The combustion efficiency,  $\eta_{C^*}$ , is defined as the ratio between the experimentally measured characteristic exhaust velocity,  $C^* = (P_{aft} \cdot A_{throat}) / (\dot{m}_{ox} + \dot{m}_{fuel})$ , to the theoretical one; the latter has been computed with the CEA chemical equilibrium code [15] at the effective mean pressure ( $P_{aft}$ , measured in the aft-mixing chamber) and mean mixture ratio:

$$\frac{O}{F} = \frac{\dot{m}_{ox}}{\dot{m}_f} \quad (7)$$

## 4. Experimental Results

In this section results obtained in the present firing test campaign are discussed and compared with some relevant data in the literature. Furthermore, regression rates achieved in the framework of ORPHEE project with aluminium-loaded HTPB grains are recalled and shown against current data.

First, pure HTPB/nitrous oxide firing results obtained both with the small and the large scale motors are examined and compared with the data achieved with oxygen; then focus is put on the effect of additives. Finally, results with paraffin-based fuels are discussed.

### 4.1 Carbon black or Aluminum-loaded HTPB solid fuels

In this test campaign pure HTPB (as a baseline), HTPB with carbon black, and aluminum-loaded HTPB fuel grains have been burnt, with nitrous oxide. Grains have been manufactured by AVIO with the following four formulations

1. No additives, e.g. pure HTPB used as a reference fuel.
2. Carbon-black powder additive, (CB)
3. Nano-sized aluminum powder additive, Alex (n-Al) (average particle diameter 0.1  $\mu\text{m}$ )
4. Micro-sized aluminum powder additive, Alex type (1) (average particle diameter 6.5/8  $\mu\text{m}$ )

Pure HTPB grains have been tested to check the test facility and to make a reference in terms of fuel performance. In Table 1 fuel composition is reported.

**Table 1: Loaded HTPB grain formulations**

	<b>HTPB</b>	<b>Carbon black</b>	<b>nanoAl</b>	<b>Al type 1</b>
HTPB+CB	76.6 %	3%	-	-
HTPB+nanoAl	76.6%	-	3%	-
HTPB+Al 1	76.6%	-	-	12.8%

In each composition the residual fuel fraction (i.e. around 10%-20%) is constituted by a plasticiser.

The average parameters measured over the burning tests are reported in Table A1 (data relevant to the 0.2-kN-thrust motor) and in Table A2 (data relevant to 1-kN thrust motor).

Tests with pure HTPB grains have been carried out on both scales rocket engines with the aim to assess possible scales effects.

The basic concept behind the test matrix was to perform a series of tests on pure HTPB with a total mass flux in the range of 50-250 kg/m<sup>2</sup>s. This test series includes two different initial port diameters, 12 mm and 25 mm (see Table A1). Firing setting parameters, that are nitrous oxide feeding pressure (i.e. oxidizer mass flow), and burning time have been chosen accordingly; different port final diameters have been achieved, which allows studying the geometrical effect of the port diameter on the fuel regression rate.

Tests conducted on the larger-scale motor have been organized in the same range of mass fluxes and similar pressure, but with a unique initial port diameter of 25 mm.

Tests with aluminum-loaded grains have been planned with the same oxidizer feeding pressure and burning duration as the ones with pure HTPB in order to observe the difference in regression rate. In particular, for each additive, three tests have been planned for comparison with test n° 4, 5 and 6 with pure HTPB (see Table A1 and Table A2).

In Figure 5 the pressure-time trace of test n° 2 has been reported. In the same picture also the nitrous oxide mass flow rate and thrust are plotted.

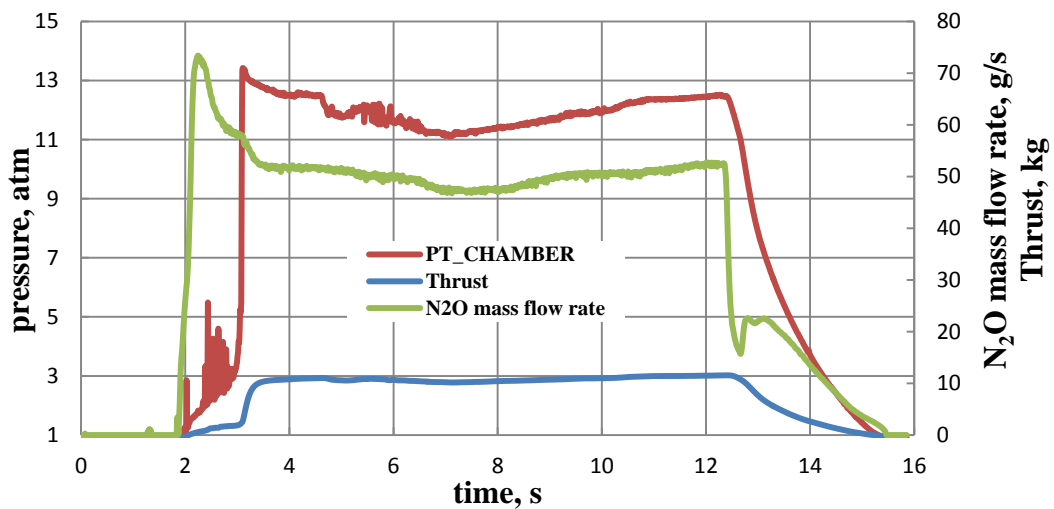


Figure 5: Pressure, nitrous oxide flow rate and motor thrust vs. time for Test n° 2

The same plots for test n° 4 are depicted in Figure 6 for comparison. These diagrams have been represented because they are typical of burning tests with small and large port diameters (compared to the oxidizer jet diameter at the entrance of the fuel grain), respectively.

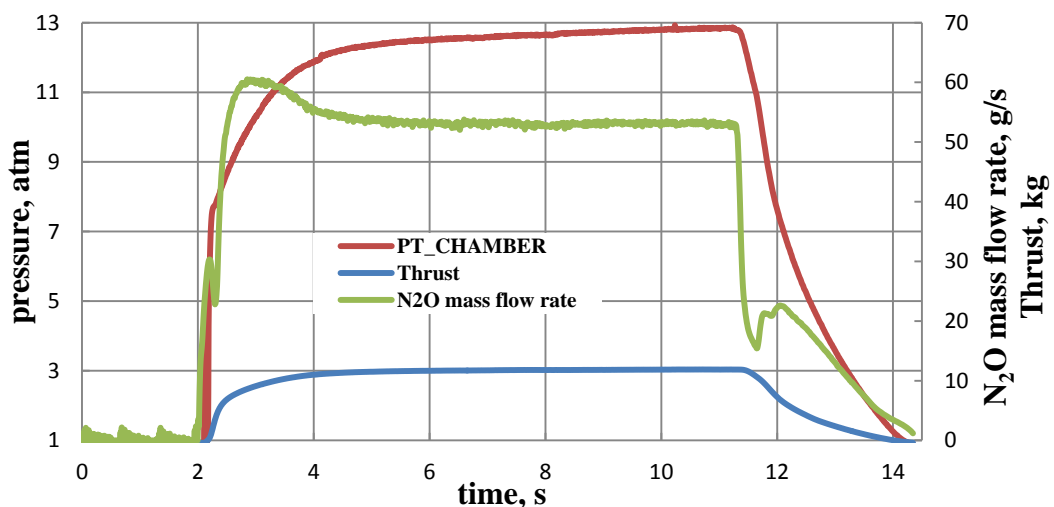


Figure 6: Pressure, nitrous oxide flow rate and motor thrust vs. time for Test n° 4

As can be seen in Figure 6, combustion chamber pressure in test n° 4 is globally smoother than the one of test n° 2, and shows a slightly increasing profile over the firing. In fact, if the initial port diameter is small compared to the oxidizer jet at the grain entrance, pressure displays an initially decreasing trend over time (as expected in a hybrid system in which fuel mass flow rate decreases over the burn due to the port opening), followed by an increase consequent on the oxidizer jet penetration inside the combustion port, which produces an increase of regression rate. This phenomenon confirms that there is a significant effect of the recirculation induced at the head end of the port by the oxidizer injection [11][16] and has been observed also on the larger-scale motor fed by oxygen and several other fuels [3][16].

Moreover, pressure-time traces of tests carried out on the larger motor (fed with N<sub>2</sub>O) show a quite smooth and increasing trend as can be observed in Figure 7, where data from test n° 20 have been selected as an example.

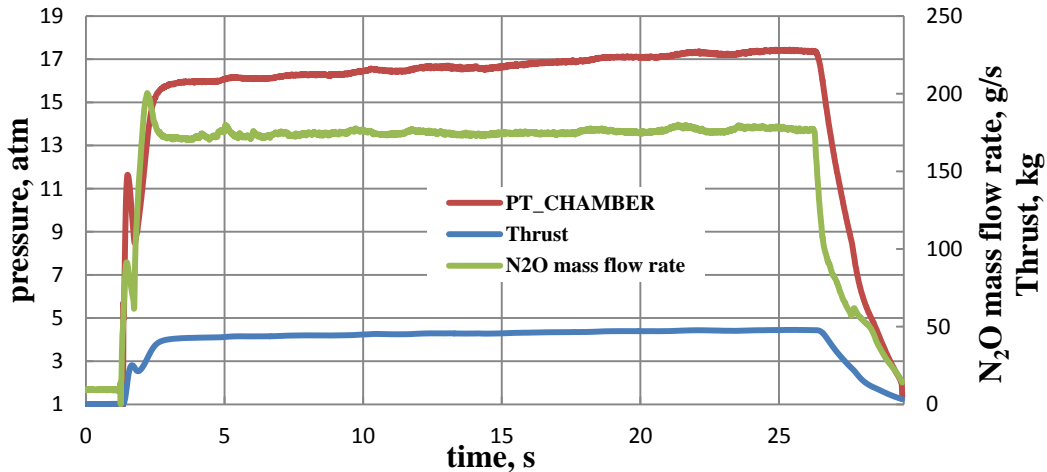


Figure 7: Pressure, nitrous oxide flow rate and motor thrust vs. time for Test n° 20

In Figure 8 the average regression rate obtained with pure HTPB grains is plotted as a function of the oxidizer mass flux. The experimental points in the graph have been retrieved in this test campaign from both the small and large scale engines. The main purpose of this comparison is the assessment of a possible scale effect on the regression rate. Figure 8 shows that no noticeable influence of the motor scale can be unveiled. However, the main parameter that significantly changes from the small-scale motor to the large-scale one is the grain length, which, in the larger scale motor, is around the double of the small-scale one. This feature, at given oxidizer fluxes, only implies lower overall oxidizer-to-fuel ratios in the larger-scale motor (for the larger fuel mass flow rate); the latter parameter, thus, shows no major effect on the regression rate according to the diffusion-limited theory.

In the same diagram a trend line (black dotted line) calculated from some data available in the open literature is overlapped. These data have been obtained through a series of scale-up tests with gaseous nitrous oxide carried out at Stanford University in the framework of MATADOR project (see [17]). Note that the laboratory rocket used over this latter project is almost of the same size as the current one. Initial port diameter is around 19-22 mm (i.e. very close to the one employed in this test campaign), while grain length is in the range of 127-230 mm. Oxidizer to the fuel ratios are, indeed, comparable to the ones measured with the small-scale engine.

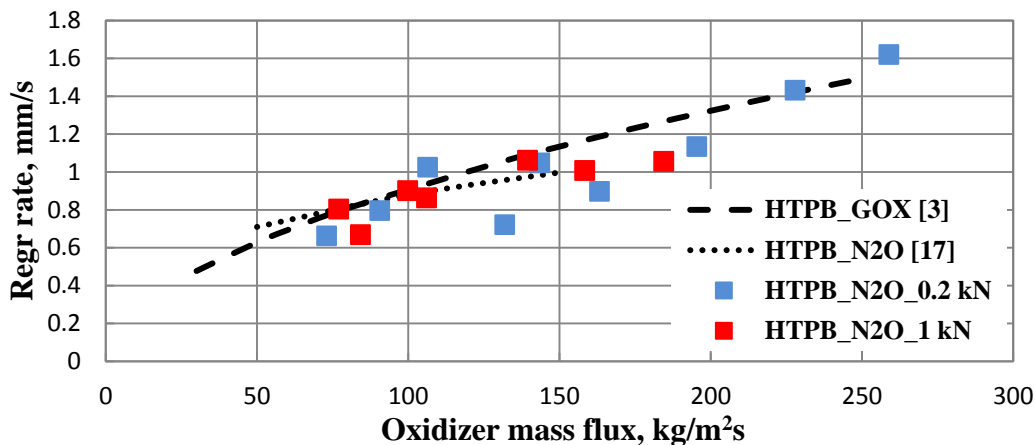


Figure 8: Average regression rate as a function of the oxidizer mass flux

Finally, on the same picture regression rates achieved from burning pure HTPB with gaseous oxygen in the large-scale hybrid rocket [3] have been reported.

Regression rate of pure HTPB grains burnt with nitrous oxide in this firing campaign is in fairly good agreement with that retrieved from literature. In conclusion, from a comparison amongst all the aforementioned data, no significant difference between regression rates of HTPB grains can be evidenced either if they are burnt with nitrous oxide or oxygen.

The following picture shows chamber pressure vs time for test n° 11 carried out with nAl-loaded HTPB. Also in this case a very smooth behaviour is displayed. This is a very interesting feature, because nano-aluminum loaded HTPB grains burned with gaseous oxygen on the large scale motor have shown very large pressure oscillations with a dominant frequency around 5 Hz (see [3]). In that case, the hypothesis was that unburned aluminum oxide particles agglomerated on the nozzle throat due to its low temperature (water cooled copper nozzle) and induced the observed very low-frequency instability. This concept may be, actually, supported by the fact that current firings have been performed with graphite nozzles and in no cases pressure oscillations have been detected.

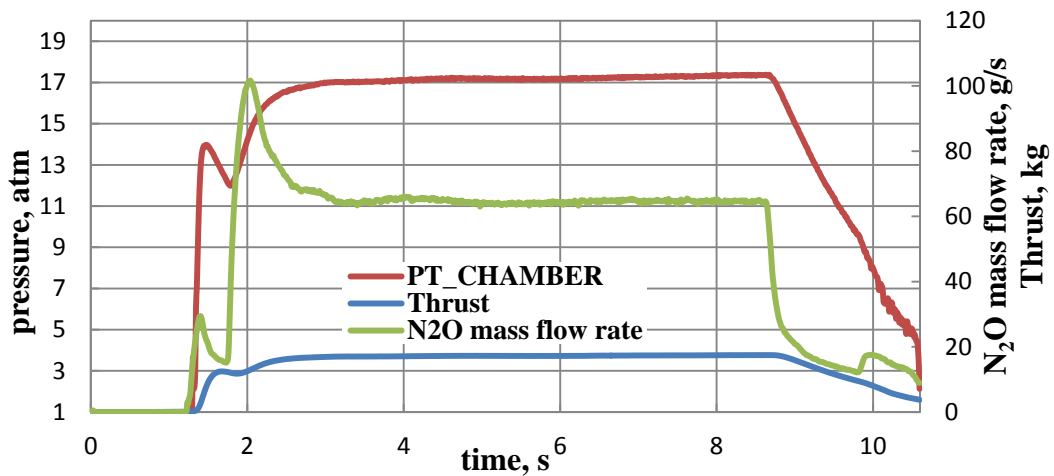


Figure 9: Pressure, nitrous oxide flow rate and motor thrust vs. time for Test n° 11 with nAl -loaded HTPB

The effect of additives on the fuel regression rate can be observed in Figure 10 in which regression rates of HTPB grains containing carbon black or aluminum powders are compared with the one of pure HTPB burnt with nitrous oxide.

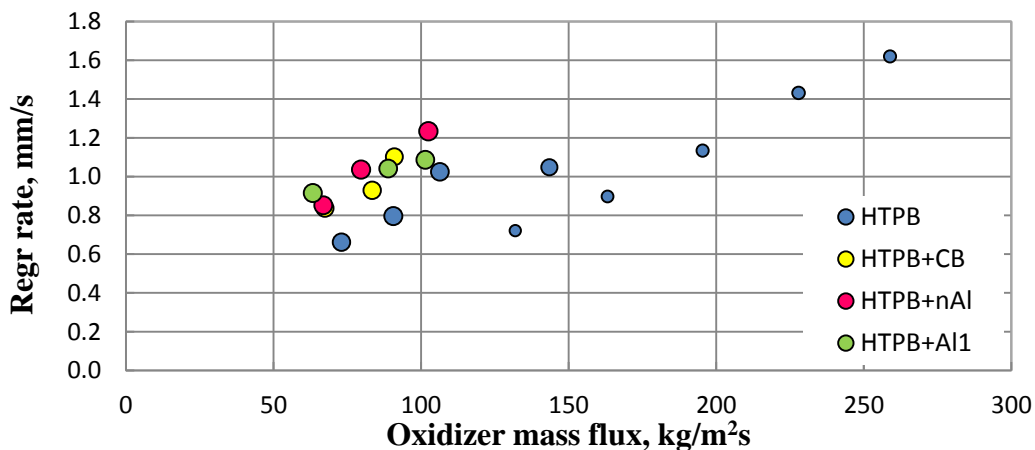


Figure 10: Average regression rate as a function of the nitrous oxide mass flux; bubbles refer to average port diameters

In the same diagram the influence of the port diameter on pure HTPB regression has been highlighted; in fact, data points have been represented with their size proportional to the average port diameter. As already demonstrated (refer to [2],[3] and [16]), at the same mass flux, grains with larger port diameter exhibit faster regression due to the higher heat transfer to the wall caused by the oxidizer recirculation into the port. Note that tests n° 4-5-6 carried out with pure HTPB at low mass fluxes (73-106 kg/m<sup>2</sup>s) are assumed as the baseline for the assessment of the effect of additives.

Tests with particle-loaded HTPB grains seem to confirm the benign influence of the additives on the regression rate. In Figure 11 the regression rate increase due to additives is analysed for each mass flux in comparison to tests n° 4-5-6. Bars (and data points in Figure 10) are coloured based on the specific additive as described in the legend of Figure 11. Note that through all the tests analysed the average port diameter is almost the same (around 30-32 mm) which allows eliminating the influence of the port diameter itself.

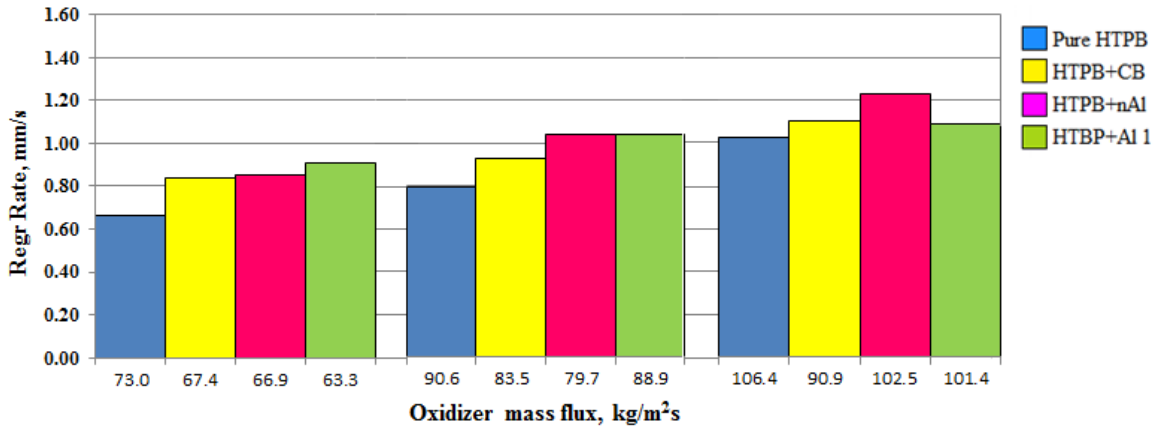


Figure 11: Average Regression Rate of particle loaded HTPB compared to pure HTPB

At similar mass fluxes, HTPB grains with carbon black display moderately higher regression rate as also observed in some literature data [18]. Actually, carbon black is an opacifying agent generally adopted as additive to the solid grain in order to increase its absorptivity. Thus, the gain in regression rate due to the carbon black can be attributed to an increase of the radiation heat transfer for both the improved properties of the fuel (a sort of "black body" effect) and the radiant heat feedback from carbon particles ejected off the grain. However, some other data show that the addition of carbon black has no effect on regression behaviour [19].

Aluminum powder addition results in a slightly more marked regression rate improvement. With all the three levels of oxidizer fluxes examined, aluminium-loaded grains (both nano-sized and micro-sized aluminum) burnt with regression higher than the one achieved with pure HTPB and HTPB with carbon black. No significant difference can be observed between the regression rates obtained with the two aluminium powders (and mass fractions). The highest regression rate increase, i.e. around 40%, is achieved with micro-aluminum at the lowest mass flux (around 60 kg/m<sup>2</sup>s), while at the intermediate mass flux (around 80 kg/m<sup>2</sup>s) both nano-aluminum and micro-aluminum loaded-HTPB show about 31% increase.

Finally, Figure 12 reports the regression rates measured in this campaign with both pure HTPB and aluminium-loaded HTPB in comparison to results obtained in the ORPHEE program [3] by burning pure (dashed line) or metal-loaded HTPB (black or blue circles) with gaseous oxygen. Pure HTPB/nitrous oxide regression rate data have been represented by means of a trend blue line (computed from the data reported in Figure 10).

It is worth noting that regression improvement (over the pure fuel) observed in this test campaign is larger than the one achieved in ORPHEE by burning aluminium-loaded HTPB on the large-scale motor.

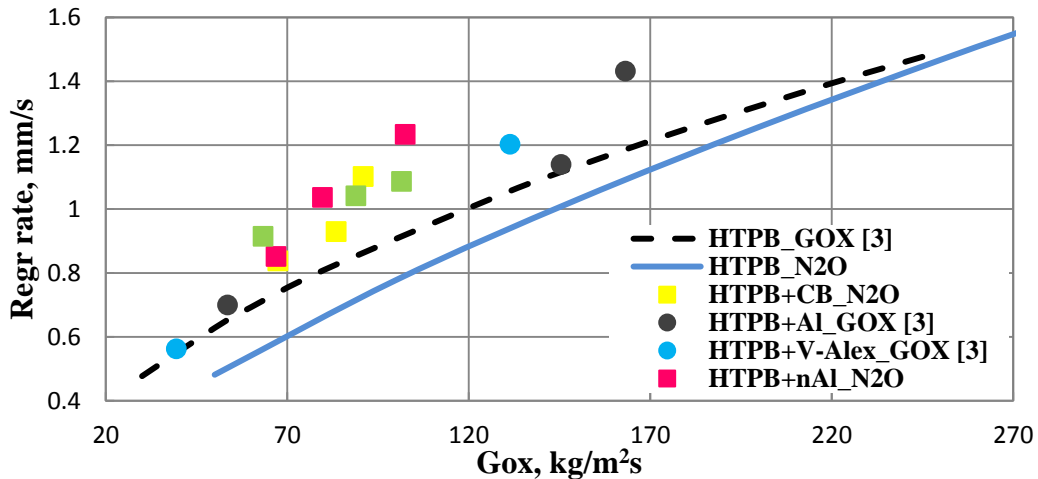


Figure 12: Particle loaded HTPB average regression rate as function of oxidizer mass flux

## 4.2 Paraffin-based fuel

The paraffinic fuel grains burnt in this test campaign have been produced at SPLab of Politecnico di Milano [13]. The fuel grain formulation consists of about 84% solid wax (SW, i.e. solid paraffin-wax), about 15% SEBS and carbon black (about 1%). The SW has a melting point of 333 K.

SEBS is a thermoplastic polymer belonging to the family of Styrene-Butadiene rubbers (SBR) with styrene content of about 30%. This thermoplastic polymer offers a good chemical compatibility with paraffinic materials. This characteristic ensures that a homogeneous formulation is obtained.

The average parameters measured in the burning tests are reported in Table A3. Nitrous oxide feeding pressure and burning duration have been chosen with the aim to achieve an average oxidizer mass flux comparable to the results obtained with metal-loaded HTPB. Tests carried out with paraffin-based fuels show pressure oscillations, as can be noticed in Figure 13. This pressure behaviour is quite similar in tests SW\_02 and SW\_03 and it is common to a lot of experimental data found in the literature with same propellants. In one test, very large pressure spikes (negative to positive pressure variation) have been observed at the early phase of combustion. This behaviour is probably due to some chunks of fuel produced at the grain inlet.

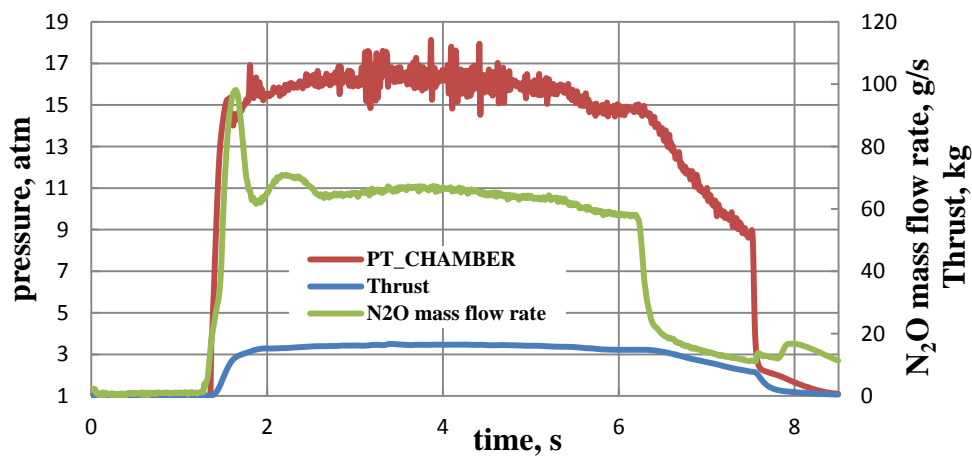


Figure 13: Pressure, nitrous oxide flow rate and motor thrust vs. time for Test n° SW\_05

All grains, indeed, have been subject to a loss of fragments that, in two cases (test SW\_02 and SW\_03), led to the graphite nozzle failure. The divergent portion of the nozzle has been broken off when chunks have been expelled from the nozzle itself.

Paraffin fuel chunks are generated as a consequence of grain poor mechanical properties; low stiffness can be due to the low casting temperature that inhibits the breakdown of the maleic anhydride molecule, which is an intrinsic component of SEBS. This molecule at high temperature is brought to break its characteristic ring structure creating strong chemical bonds with the consequent improvement of the polymer mechanical properties. This phenomenon has been observed when casting previous grains burned with oxygen, for which higher temperature has been achieved as well as larger stiffness.

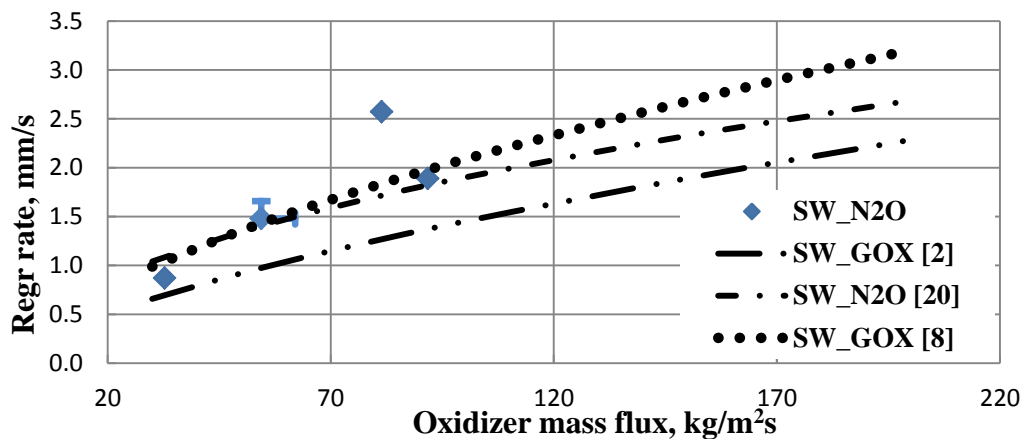


Figure 14: Comparison between average regression rates obtained with paraffin-based fuels and nitrous oxide and the ones achieved with gaseous oxygen

Fuel fragments production can influence also the regression rate measurement. In fact, regression rates measured in this study, compared with data obtained burning gaseous oxygen [2] and swirling nitrous oxide [8], appear larger than expected, as shown in Figure 14. However, three out of four data points are in line with the regressions of SW/GOX. Test SW\_02 (oxidizer flux around 60 kg/m<sup>2</sup>s) is one of the tests affected by nozzle failure; in this case failure occurred in the middle of the firing; thus regression rate measurement has been estimated only on the first portion of the test, prior to failure; the measurement uncertainty has been consequently evaluated and reported with the relative error bars. Whereas the point around 80 kg/m<sup>2</sup>s (relevant to test SW\_05) was affected by a major grain failure and appears definitely out of range.

### 4.3 Fuel performance

In this section regression rates gathered from all the several fuel formulations (basically pure HTPB, aluminum-loaded HTPB and paraffin-wax) tested in this and in previous experimental campaigns are compared. In Figure 15 data are reported as function of the oxidizer mass flux (either gaseous oxygen or nitrous oxide).

It is clear that aluminium powder addition to HTPB has a positive effect on regression rate, both with oxygen and nitrous oxide. Aluminized HTPB burnt with nitrous oxide, in the range of fluxes and pressures tested, show a regression rate increase which is not appreciably sensitive to either aluminium particles mass fraction or size. Moreover, it seems that aluminium improves the regression of HTPB more effectively if burnt with nitrous oxide than with oxygen. In fact, aluminium-loaded HTPB with nitrous oxide seems to regress even faster than the same fuel burnt with oxygen. A possible reason can be related to the flame adiabatic temperature increase due to the aluminium addition. Temperature increase, in the range of mixture ratios expected in a hybrid rocket, for the propellant system with nitrous oxide is much higher than for the one with oxygen, indeed. Anyway, the latter outcome is not yet well understood and further investigation is needed.

Regression rates measured with paraffin-wax and nitrous oxide are the largest over all the available data. This result, even if almost aligned with literature, is affected by fuel fragments loss, as previously mentioned

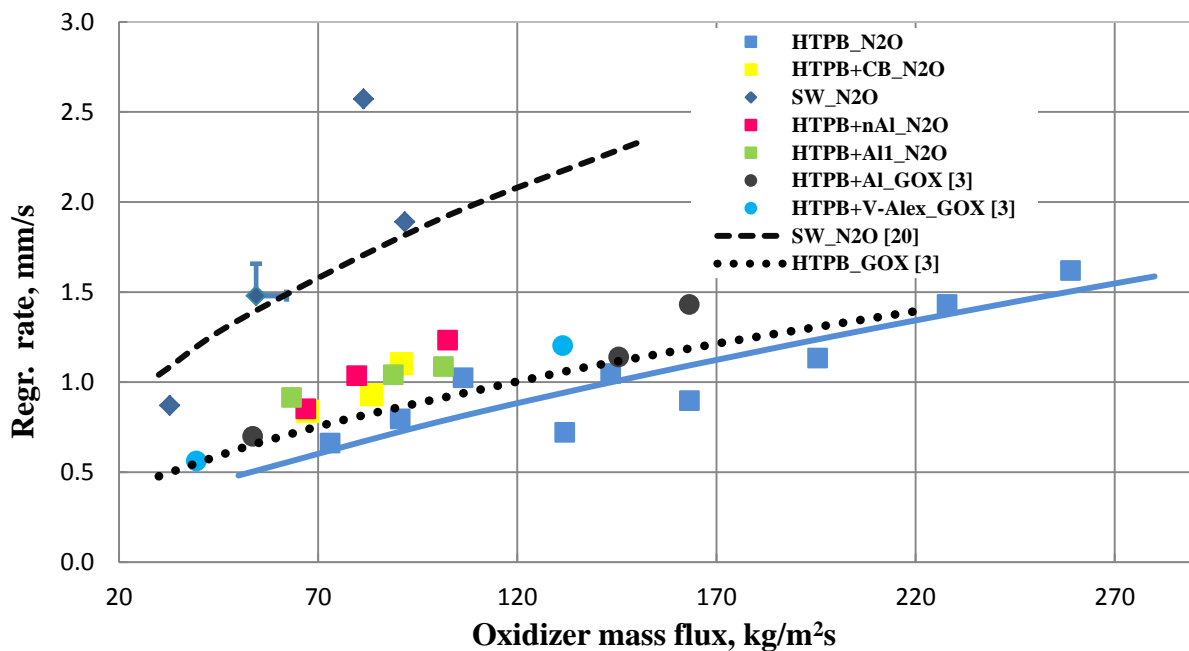


**Figure 15: Comparison between average regression rate obtained with pure and loaded HTPB fuels and the ones achieved with paraffin fuels**

Figure 16 shows a couple of pictures of the solid fuel grain before and after the burning in test SW\_05. It is clear that, in the head end region of the grain, a failure was present leading to loss of fragments.



Figure 16: Detail of solid-wax grain burned in test SW\_05: a) before firing; b) after firing

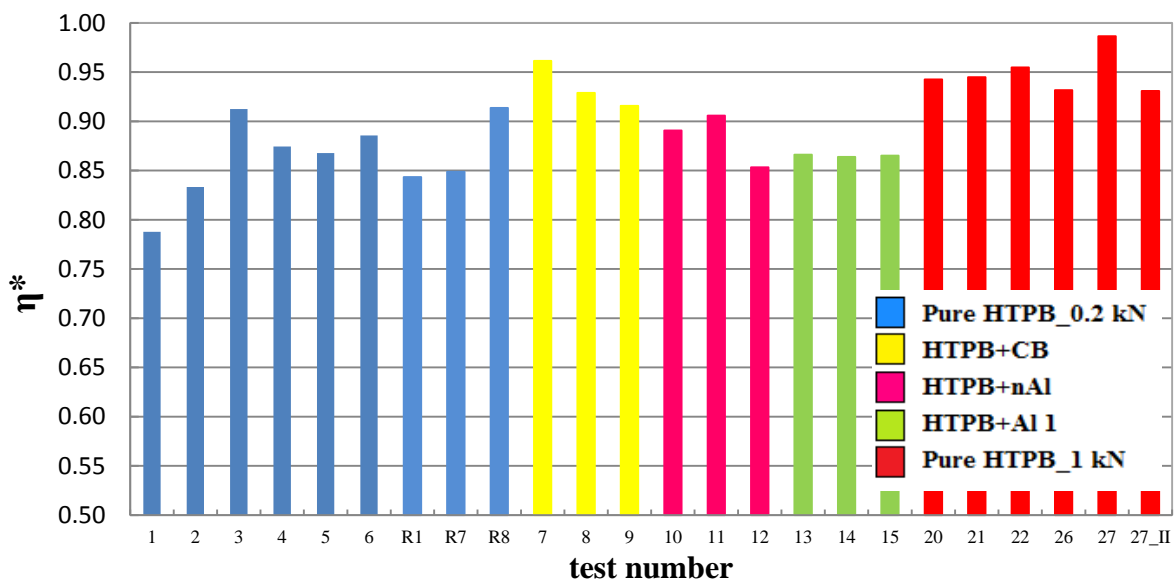


Figure 17: Combustion efficiencies calculated for pure and loaded HTPB

In Figure 17 combustion efficiencies computed for all HTPB-based fuel grains have been reported. The efficiency ranges from 78% to a maximum value of 98%. Significantly high values of combustion efficiencies have been also obtained with HTPB and gaseous oxygen [3].

It is remarkable that, by comparison between data relevant to pure HTPB burned in the small- and large-scale motors, combustion efficiency in the larger motor is, on average, higher than in the smaller-scale motor, as expected from the large difference in the motor characteristic length values; large-scale motor characteristic length is about 160% greater than the small-scale one.

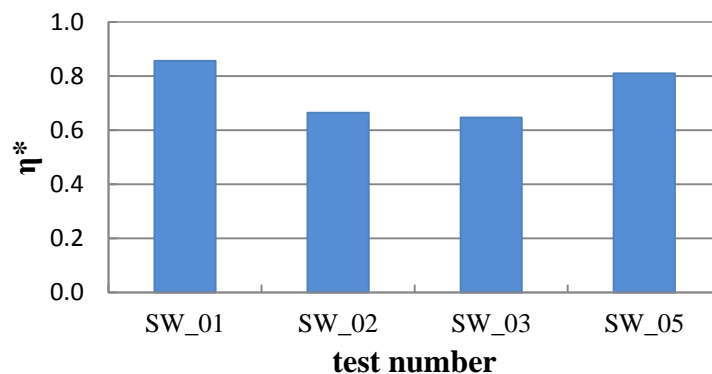


Figure 18: Combustion efficiencies with solid wax fuel

---

Figure 18 depicts combustion efficiency measured with paraffin-wax grains. Efficiency of paraffin grains is considerably lower than the one of HTPB-based fuels. The maximum value achieved over the four tests is 86%. Lower efficiency is expected when burning paraffin grains due to the higher fuel flow rate which does not burn in the combustion chamber [2], but in this case these values probably appear even lower than in reality because of the anomalous behaviour of the solid grains (fragments loss).

However, it is clear that during the firing test non negligible amount of liquid paraffin is generated, entrained in the main flow and transported back to the injection region (due to the broad recirculation head of the combustion port), where it is deposited on the injection flange, as demonstrated by post-firing inspections. This issue has been observed also with oxygen in the small motor [2]. In addition, unburned fuel was found on the thermal protections covering the aft-mixing chamber. Of course, fuel slivers are not consumed during combustion, and do not contribute to raise the combustion chamber pressure, thus lowering the efficiency.

## 5. Conclusion

In this paper, two of the strategies applied to raise hybrid fuel regression-rate are approached: addition of energetic materials to conventional HTPB fuel and use of liquefying paraffin fuels. A comparison between regression rates achieved by burning gaseous nitrous oxide injected axially with a shower-head injector in single-port grains of pure HTPB, HTPB loaded with aluminum particles, and paraffin-based fuels, has been drawn.

The results obtained from a lab-scale engine firing campaign show that grains of HTPB loaded with aluminium particles regress somewhat faster independently from the aluminium size and mass fraction (3% of micro-sized or 12.8% of nano-sized particles). The regression rate increase is about 25% at 100 kg/m<sup>2</sup>s.

Further regression rate improvement (around 90% at 100 kg/m<sup>2</sup>s) is shown by paraffin-based fuel. Unfortunately, regression rate measurement accuracy has been degraded for the loss of grain fragments over the burning. This shortcoming is a consequence of the grains manufacturing process which has been devoted to the regression improvement at the expense of the propellant mechanical performance. Also the combustion efficiency has been lowered compared to other fuels tested.

However, current test campaign has confirmed a strong influence of the grain manufacturing process on the paraffin-fuel firing results.

## Acknowledgments

Research leading to these results has received funding from MIUR in the frame of PRIN 2009 and from ASI in the frame of THESEUS Program.

Special thanks to Ing. Bruno Alfano for his support.

## References

- [1] Marxman, G.A. and M. Gilbert.1963. Turbulent boundary layer combustion in the hybrid rocket. In: *9<sup>th</sup> International Symposium on Combustion, Academic Press* pp 371-383.
- [2] Scaramuzzino, F., G. Festa, C. Carmicino and A. Russo. 2012. Hybrid-rocket motor performance trade off with paraffin based and metal-loaded HTPB fuel grains. In: *63rd International Astronautical Congress*.
- [3] Carmicino, C., A. Russo Sorge, O. Orlandi, H. Blanchard, P. Yvart and P. Gautier. 2012. Lab-scale Motor Firing Results on Advanced Solid Fuels for Hybrid Propulsion. In: *AAAF-ESA-CNES Space Propulsion*.
- [4] Risha, G.A., B.J. Evans, E. Boyer and K.K. Kuo. 2007. Metals, Energetic Additives, and Special Binders Used in Solid Fuels for Hybrid Rockets, Fundamentals of Hybrid Rocket Combustion and Propulsion. In: *Progress in Astronautics and Aeronautics, AIAA*. Vol.18. pp. 423-442.
- [5] Strand, L.D., R.L. Ray and N.S. Cohen. 1993. Hybrid Rocket Combustion Study. In: *29<sup>th</sup> Joint Propulsion Conference, AIAA/SAE/ASME/ASEE*. AIAA paper 93-2412.
- [6] Netzer, D.W. 1972. Hybrid Rocket Internal ballistics. CPIA Publ. n.222.
- [7] Martin, F., A. Chapelle, O. Orlandi and P. Yvart.2010.Hybrid Propulsion Systems for Future Space Applications. In: *46<sup>th</sup> AIAA/ASME/SAE/ASEE Joint Propulsion Conference & Exhibit*. AIAA paper 2010-6633
- [8] Karabeyoglu, M.A., D. Altman and B.J. Cantwell. 2002. Combustion of liquefying hybrid propellants: Part 1 General Theory. *Journal of Propulsion and Power*. Vol. 18, n.3.
- [9] Gater, R.A. and M.R.L. L'Ecuyer. *A fundamental investigation of the phenomena that characterize liquid film cooling*. *International Journal of Heat and Mass transfer*. 1970. 13(3): 1925-1939.
- [10] Karabeyoglu, M.A., G. Zilliac, B.J. Cantwell, S. DeZilwa.2003.Scale-up tests of high regression rate liquefying hybrid rocket fuels.In: *41<sup>st</sup> Aerospace Sciences Meeting and Exhibit*. AIAA 2003-1162.
- [11] Carmicino, C. 2009. Acoustic, Vortex Shedding, and Low-Frequency Dynamics Interaction in an Unstable Hybrid Rocket. *Journal of Propulsion and Power*. Vol. 25, n.6.
- [12] Merotto, L., M. Boiocchi, A. Mazzetti, F. Maggi, L. Galfetti, L.T. De Luca. 2012. Characterization of a Family of Paraffin-based Solid Fuels. In: *EUCASS 2011*.
- [13] Boiocchi, M., 2012. Innovative fuel formulations for hybrid rocket engines: mechanical and ballistic characterization. *PhD Thesis*. Politecnico di Milano.
- [14] Carmicino, C., A. Russo Sorge. 2005. Role of Injection in Hybrid Rockets Regression Rate Behaviour. *Journal of Propulsion and Power*. Vol. 21, n.4. pp. 606-612.
- [15] Gordon, S., B.J. McBride, Computer program of complex chemical equilibrium compositions and applications. 1994. *NASA Reference Publication 1311*.
- [16] Carmicino, C. A. Russo Sorge. 2006. Influence of a Conical Axial Injector on Hybrid Rocket Performance. *Journal of Propulsion and Power*. Vol. 22, n.5.
- [17] Lohner, K., J. Dyer, E. Doran, Z. Dunn, G. Zilliac. 2006. Fuel Regression Rate Characterization Using a Laboratory Scale Nitrous Oxide Hybrid Propulsion System. In: *42<sup>th</sup> Joint Propulsion Conference, AIAA/SAE/ASME/ASEE*. AIAA paper 2006-4671.
- [18] Cauty, F., C. Eradès. 2000.Effect of the carbon black powder on HTPB regression rate. In: *International Conference on High Energy Materials & Exhibit – HEMCE*.
- [19] Chiaverini, M.J., N. Serin, D. K. Johnson, Y. Lu. 1997. Instantaneous Regression Behavior of HTPB Solid Fuels Burning with GOX in a Simulated Hybrid Rocket Motor. In: *International Journal of Energetic Materials and Chemical Propulsion*. Vol. 4. pp. 719-733.
- [20] Bellomo, N., M. Faenza, F. Barato, A. Bettella, D. Pavarin, A. Selmo. 2012. The “Vortex Reloaded” project: experimental investigation on fully tangential vortex injector in N<sub>2</sub>O-paraffin hybrid motors. In: *48<sup>th</sup> Joint Propulsion Conference, AIAA/SAE/ASME/ASEE*. AIAA paper 2012-4304.

## Appendix

Table A1: Firing results HTPB/N<sub>2</sub>O class of thrust motor 0.2 kN

Test	Fuel comp.	L [mm]	D <sub>0</sub> [mm]	G <sub>ox</sub> [kg/m <sup>2</sup> s]	OF	G <sub>tot</sub> [kg/m <sup>2</sup> s]	$\dot{m}_{ox}$ [kg/s]	P <sub>c</sub> [bar]	$\bar{r}$ [mm/s]	$\bar{D}$ [mm]	C* [mm/s]	$\eta_{C^*}$	P <sub>feed</sub> [bar]	t <sub>b</sub> [s]
1	HTPB	239	11.7	131.9	3.9	165.3	0.040	8.52	0.72	19.7	1217.8	0.79	16.0	11.0
2	HTPB	238	11.7	163.2	4.1	203.4	0.053	12.07	0.90	20.4	1295.5	0.83	20.5	9.7
3	HTPB	239	11.6	195.4	4.1	243.5	0.069	17.12	1.13	21.2	1419.0	0.91	27.5	8.5
4	HTPB	240	23.7	73.0	3.8	92.4	0.052	12.26	0.66	30.1	1338.2	0.87	20.0	9.6
5	HTPB	239	23.5	90.6	3.9	113.6	0.069	16.29	0.80	31.2	1340.8	0.87	26.0	9.8
6	HTPB	239	23.7	106.4	3.5	136.8	0.078	18.61	1.02	30.5	1332.2	0.89	31.0	6.7
R1	HTPB	245	23.3	143.5	4.1	178.7	0.088	20.06	1.05	27.9	1312.3	0.84	32.0	4.4
R7	HTPB	243	11.7	258.9	3.6	330.3	0.088	20.11	1.62	20.8	1287.7	0.85	32.5	5.6
R8	HTPB	243	11.8	227.9	3.7	288.8	0.083	20.92	1.43	22.2	1396.9	0.91	32.5	6.9
7	HTPB+CB	239	23.8	67.4	2.6	93.5	0.047	12.41	0.84	29.8	1359.8	0.96	19.5	7.2
8	HTPB+CB	239	23.9	83.5	2.9	112.1	0.059	14.81	0.93	29.9	1339.4	0.93	25.0	6.5
9	HTPB+CB	240	23.8	96.0	2.7	131.3	0.061	15.54	1.11	28.7	1305.7	0.92	27.5	5.0
10	HTPB+nAl	241	23.8	66.9	2.4	95.1	0.050	12.85	0.85	30.9	1292.4	0.89	20.0	8.3
11	HTPB+nAl	241	23.8	79.7	2.6	110.4	0.063	16.89	1.04	31.6	1325.4	0.91	25.5	7.5
12	HTPB+nAl	241	23.9	102.5	2.8	138.6	0.081	20.16	1.23	31.7	1251.3	0.85	31.0	6.3
13	HTPB+AlI	239	23.8	63.3	2.2	91.9	0.048	13.50	0.91	31.2	1310.9	0.87	20.0	8.0
14	HTPB+AlI	241	23.6	88.9	2.6	122.5	0.065	17.61	1.04	30.6	1328.8	0.86	25.5	6.7
15	HTPB+AlI	240	23.7	101.4	2.9	136.1	0.075	20.60	1.09	30.7	1360.7	0.87	31.0	6.4

Table A2: Firing results HTPB/N<sub>2</sub>O class of thrust motor 1kN

Test	Fuel comp.	L [mm]	D <sub>0</sub> [mm]	G <sub>ox</sub> [kg/m <sup>2</sup> s]	OF	G <sub>tot</sub> [kg/m <sup>2</sup> s]	$\dot{m}_{ox}$ [kg/s]	P <sub>c</sub> [bar]	$\bar{r}$ [mm/s]	$\bar{D}$ [mm]	C* [mm/s]	$\eta_{C^*}$	P <sub>feed</sub> [bar]	t <sub>b</sub> [s]
RG1	HTPB	565	25.6	84.2	1.7	131.6	0.061	5.63	0.67	30.4	1184.1	0.85	10	7.3
RG2	HTPB	570	25.0	184.5	2.6	255.3	0.158	14.73	1.06	33.0	1353.6	0.93	24	7.6
20	HTPB	569	25.2	76.9	1.9	116.4	0.120	11.48	0.80	44.5	1266.6	0.93	18.5	24.0
21	HTPB	568	24.9	99.8	2.4	141.8	0.178	16.66	0.90	47.7	1316.8	0.94	26	25.2
22	HTPB	570	25.1	139.5	2.6	192.6	0.210	19.66	1.06	43.8	1353.8	0.95	31.5	17.5
26	HTPB	590	25.1	106.1	2.3	153.3	0.134	12.55	0.86	40.2	1285.5	0.93	31.5	17.4
27	HTPB	567	24.8	158.3	2.6	218.8	0.168	16.13	1.01	36.7	1397.9	0.99	26	11.9

Table A3: Firing results SW/N<sub>2</sub>O class of thrust 0.2 kN

Test	Fuel comp.	L [mm]	D <sub>0</sub> [mm]	G <sub>ox</sub> [kg/m <sup>2</sup> s]	OF	G <sub>tot</sub> [kg/m <sup>2</sup> s]	$\dot{m}_{ox}$ [kg/s]	P <sub>c</sub> [bar]	$\bar{r}$ [mm/s]	$\bar{D}$ [mm]	C* [mm/s]	$\eta_{C^*}$	P <sub>feed</sub> [bar]	t <sub>b</sub> [s]
SW_01	SW+SEBS	221	28.8	32.8	1.5	55.2	0.028	4.12	0.87	33.2	1003.2	0.86	11.5	5.7
SW_02	SW+SEBS	220	26.6	54.4	1.5	90.4	0.047	5.41	1.48	33.1	785.7	0.66	18.0	4.4
SW_03	SW+SEBS	220	25.0	91.8	1.9	139.5	0.073	12.35	1.89	31.9	806.2	0.65	28.0	3.7
SW_05	SW+SEBS	219	18.8	81.4	1.3	145.4	0.066	15.84	2.57	32.1	946.1	0.81	27.5	5.2